Lepton-Flavour Violating Muon Decays and the Mu3e Experiment

Ann-Kathrin Perrevoort

May 15 - 29, 2017

1 Muons in the Standard Model

The muon is the charged lepton of the second generation. It is about 200 times heavier than the electron with a mass of $105.658\,374\,5(24)\,\mathrm{MeV}$ [1] and decays via the weak interaction into electrons and neutrinos with a lifetime of $2.196\,981\,1(22)\,\mu\mathrm{s}$. The most dominant decay mode with a branching fraction of almost 100 % is the so-called **Michel decay** $\mu \to e\nu\overline{\nu}$. With a branching fraction of about $1.4(4)\,\%$ an additional photon is emitted $\mu \to e\gamma\nu\overline{\nu}$, and with a branching fraction of $3.4(4) \cdot 10^{-5}$ this photon converts internally to an $e^+\,e^-$ pair $\mu \to eee\nu\overline{\nu}$. The corresponding Feynman diagrams are shown in figure 1.

Muons can easily be produced in large quantities. Measurements of the Michel decay parameters of the decay $\mu \to e\nu\overline{\nu}$ are precision tests of the electro-weak theory. The latest measurements have been performed by the TWIST collaboration [2]. No deviation from the Standard Model has been found.
In the case of the anomalous magnetic moment of the muon, a discrepancy of about 3.6σ is observed between theoretical calculations and the latest measurements [3, 4]. This could hint at contributions from physics beyond the Standard Model. Nevertheless, the difference is not yet conclusive so that huge efforts are undertaken both on the experimental and theoretical side to solve this mystery.

In addition, muons are often investigated in **intensity frontier experiments** searching for New Physics phenomena at high mass scales showing up in loops and/or with small coupling strengths.

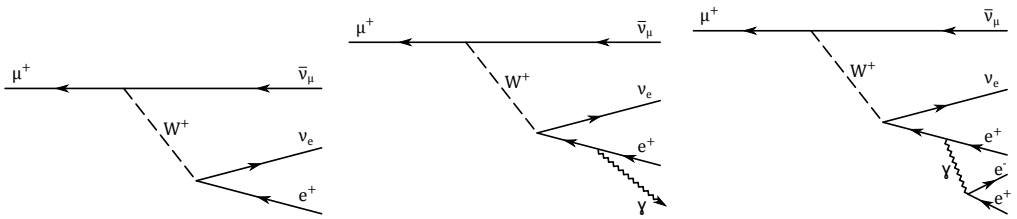

(a) $\mu \to e\nu\overline{\nu}$ (b) $\mu \to e\gamma\nu\overline{\nu}$ (c) $\mu \to eee\nu\overline{\nu}$

Figure 1: Decays of the muon in the Standard Model.

1.1 Muon Production

For the production of muons, usually a **high rate proton beam** hits a target producing amongst others a lot of **pions**. The charged pions preferentially decay into muons and neutrinos. The decay into electrons is helicity-suppressed. The muons are polarized, with μ^- from π^- decay having the spin pointing in the direction of the momentum and vice versa for μ^+ from π^+ decay.
Of particular interest are often the so-called **surface and sub-surface muons** (only μ^+). These muons stem from pions that decay at rest close to the surface of the production target. Their momentum is about 29.8 MeV in the case of surface muons and about 28 MeV for sub-surface muons. Sub-surface muons beams are used in $\mu \to e\gamma$ and $\mu \to eee$ searches. Current and future experiments of this kind are located at the Paul-Scherrer Institute (PSI) which houses an intense proton beam accelerator. Muon rates of up to $10^8 \mu/s$ of continuous beam are available at secondary beamlines. Options for rates of $10^{10}\mu/s$ are currently under study.

For the muon conversion experiments COMET at J-Parc [5] and Mu2e [6] at Fermilab pulsed muon beam in excess of $10^{10}\mu/s$ are envisaged.

2 Lepton-Flavour-Violating Muon Decays

In the Standard Model, **lepton flavour** is expected to be **conserved**. The observation of **neutrino oscillations** [1] has however taught us that lepton flavour is **violated** in nature — at least in the case of neutral leptons — and that the Standard Model is incomplete. The Standard Model extended to include neutrino masses will be referred to as νSM in the following. As neutrino flavour is violated, also the flavour of charged leptons will be violated in some order in perturbation theory. The **lepton flavour violating muon decays** are as follows: $\mu \to e\gamma$, $\mu \to eee$ and muon to electron conversion on nuclei $\mu N \to eN$. The first two will be presented in this lecture. In addition, lepton flavour violation can be investigated in muonium-antimuonium oscillations. For taus, there are more possible lepton flavour violating decays with leptons and/or hadrons in the final state.

2.1 The Decays $\mu \to e\gamma$ and $\mu \to eee$ in the νSM

The contribution to the branching ratios for $\mu \to e\gamma$ that stem from the neutrino masses and mixing alone is extremely small and by far not accessible with experiments [7–9]:

$$\mathrm{BR}(\mu \to e\gamma) = \frac{3\alpha}{32\pi}\left|\sum_{i=2,3} U^*_{\mu i} U_{ei} \frac{\Delta m^2_{i1}}{M^2_W}\right|^2 < 10^{-54}\,. \tag{1}$$

Herein, α denotes the fine structure constant, $U_{\alpha i}$ the elements of the neutrino mixing matrix, Δm^2_{ij} the differences of the squared neutrino masses, and M_W the mass of the W boson. The corresponding Feynman diagrams with neutrino mixing in a loop are shown in figure 2. The branching ratio for $\mu \to eee$ is even smaller because of the additional vertex of the photon conversion.

As the νSM contribution is negligible, $\mu \to e\gamma$ and $\mu \to eee$ are ideal probes to **search for New Physics**. Any observation would be an unambiguous signal for physics beyond the Standard Model (BSM). This is why over the past decades many experiments have been performed — so far with no signal found – and also for the future more experiments are planned pushing the sensitivity level further down (see figure 3).

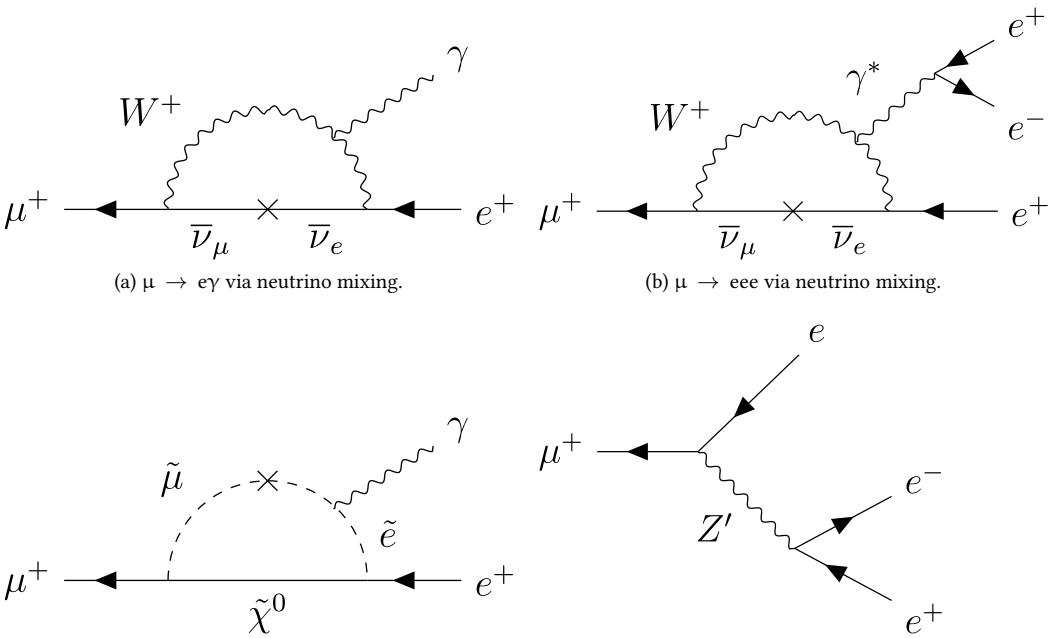

(a) $\mu \to e\gamma$ via neutrino mixing.

(b) $\mu \to eee$ via neutrino mixing.

(c) $\mu \to e\gamma$ in SUSY.

(d) $\mu \to eee$ with a Z′.

Figure 2: Feynman diagrams for $\mu \to e\gamma$ and $\mu \to eee$ mediated via neutrino mixing and in BSM.

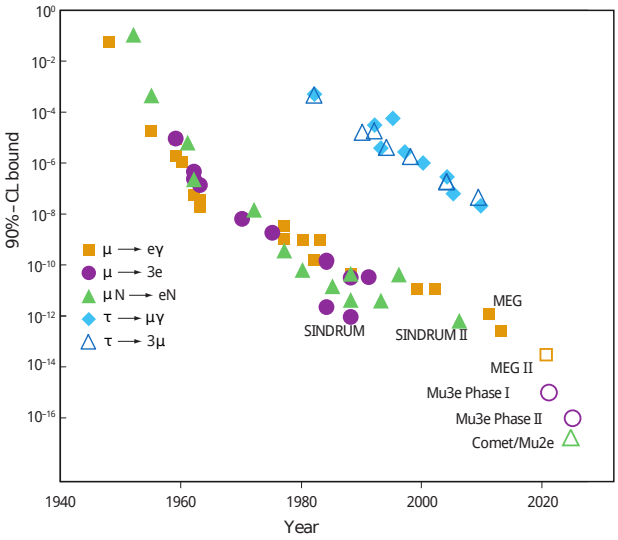

Figure 3: Past and future experiments searching for charged lepton flavour violating decays. Adapted from [10].

2.2 The Decays $\mu \to e\gamma$ and $\mu \to eee$ in BSM

Many models of New Physics predict charged lepton flavour violation at significantly enhanced rates compared to the νSM prediction of equation 1. One possibility is supersymmetric theories, but charged lepton flavour violation can also be mediated via e. g. a doubly-charged Higgs or a Z′ (see figure 2) [7, 11].

Effective field theories offer the possibility for model-independent studies. Charged lepton flavour violation is mediated by operators of dimension five or higher. The following effective Lagrangian illustrates with two exemplary operators how $\mu \to e\gamma$ and $\mu \to eee$ can be mediated [7]. More detailed considerations can be found in [11] and [12].

$$\begin{aligned}\mathscr{L}_{\text{cLFV}} =& \frac{1}{(\kappa+1)}\frac{m_\mu}{\Lambda^2}\overline{\mu}_R\sigma_{\mu\nu}e_L F^{\mu\nu} + h.c. \\ &+ \frac{\kappa}{(\kappa+1)}\frac{1}{\Lambda^2}\overline{\mu}_L\gamma_\mu e_L(\overline{e}\gamma^\mu e) + h.c.\end{aligned} \tag{2}$$

μ and e are the fermion fields with chiralities L and R, and $F^{\mu\nu}$ the photon field strength. The parameter Λ is the effective mass scale of the new degrees of freedom. And κ defines the relative size of the two operators.

The first term in equation 2 is a **dipole-type** operator. $\mu \to e\gamma$ is directly mediated via this operator, while $\mu \to eee$ is mediated at order α. The second term is an operator of **four-fermion interaction**. It mediates $\mu \to eee$ at tree level and $\mu \to e\gamma$ at one-loop level.

Figure 4 shows the sensitivity to the effective mass scale Λ as a function of κ for various limits on the branching ratio of $\mu \to e\gamma$ and $\mu \to eee$. In general, the expected branching ratio for decay experiments scales with Λ^{-4} meaning in order to investigate one more order in magnitude in mass scale, the sensitivity has to be improved by four orders of magnitude.

In the case of dominating dipole-like interaction (small κ), measurements of $\mu \to e\gamma$ excluded already effective mass scales up to more than 2000 TeV and future experiments will probe up to 4000 TeV. $\mu \to eee$ searches have to be about two orders of magnitude more sensitive to be competitive with $\mu \to e\gamma$ searches in the case of dipole-like operators. On the other hand, $\mu \to eee$ searches dominate the limits on Λ in the case of four-fermion interactions (large κ). Current results exclude mass scales up to a few hundred TeV, and future experiments are sensitive to mass scales of more than 1000 TeV.

This simple comparison between $\mu \to e\gamma$ and $\mu \to eee$ also shows that a single channel can only provide limited information about the underlying New Physics. In the case of a positive signal in $\mu \to eee$, the distribution of the decay electrons could provide some information of the type and chirality of the operators [11]. But only the combination of various observables — not only from charged lepton flavour violation, but also for example from muon (g-2) measurements and neutrino experiments – can give a more complete picture.

2.3 The Decay $\mu \to e\gamma$

The latest results on lepton flavour violation searches of muons stem from the $\mu^+ \to e^+\gamma$ decay. As it is a **two-body decay**, it has a distinct signature. Ususally, muon decays at rest are observed. One searches for a positron and a photon with an energy of half the muon rest mass (about 52.83 MeV). Both particles are emitted in a back-to-back topology, have a common vertex, and appear coincidently.

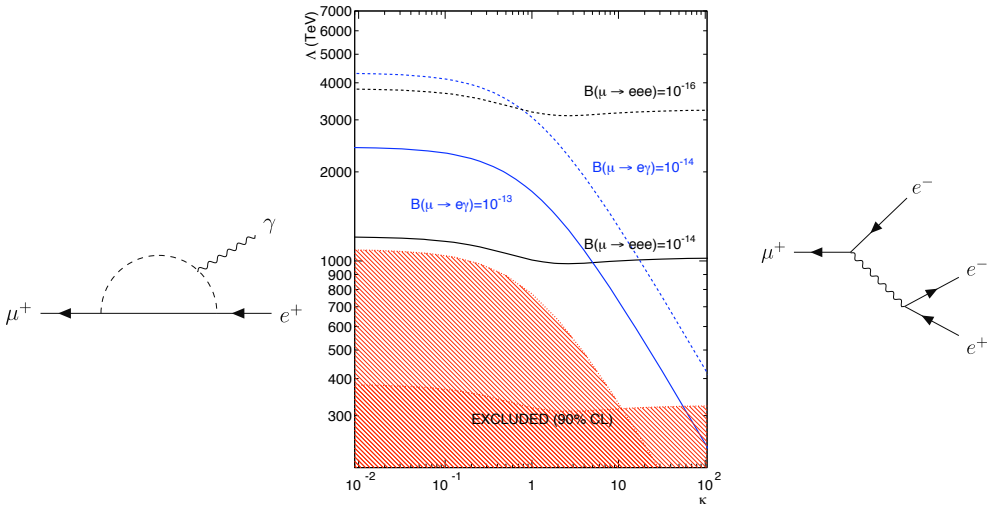

Figure 4: Comparison between $\mu \rightarrow e\gamma$ and $\mu \rightarrow eee$ in effective theories [7].

One source of **background** is the Standard Model decay $\mu \rightarrow e\gamma\nu\overline{\nu}$. The neutrinos are not detected, thus a positron and a photon from a common vertex are observed. Nevertheless, the two particles do not fully match the criteria on energy and the back-to-back topology. The energy and spatial resolution must be good enough to suppress this background.
In order to achieve competitve sensitivity levels with a reasonable measuring time, $\mu \rightarrow e\gamma$ experiments have to run a high muon rates. Thus, not single but multiple muon decays are observed at a time giving rise to accidental background, i. e. combinations of photons from $\mu \rightarrow e\gamma\nu\overline{\nu}$, Bremsstrahlung or positron annihilation with positrons for example from the dominant $\mu \rightarrow e\nu\overline{\nu}$ decay. Hence, in addition timing resolution becomes important to suppress accidental background.

The most recent result on $\mu \rightarrow e\gamma$ is set by the **MEG experiment** [13, 14] which was operated at the Paul-Scherrer Institute until 2013. The detector is shown in figure 5. A muon beam of about $3 \cdot 10^7\,\mu/s$ is stopped on a target in the centre of the experiment. For the momentum measurement of the positrons, a special magnetic gradient field is applied that ensures a nearly constant bending radius which only weakly depends on the emission angle. The positrons are tracked in a drift chamber system and their time is measured with a timing counter system made of scintillating bars. The photons are measured in a liquid Xenon calorimeter read out by photo-multiplier tubes.
A total of $7.5 \cdot 10^{14}$ muons has been stopped in the MEG experiment. The data set is analysed in a combined blind and maximum likelihood analysis (see figure 6). The sidebands are used to derive estimates for accidental background and background from $\mu \rightarrow e\gamma\nu\overline{\nu}$, before the analysis window is opened. No significant excess was found. The final result as published in 2016 excludes the decay $\mu^+ \rightarrow e^+\gamma$ to branching ratios of $BR < 4.2 \cdot 10^{-13}$ at 90% confidence level [14]. It is currently the most stringent bound in charged lepton flavour violating decays.
Figure 7 shows the distribution of events in the observables energy of photon and positron, time difference, and opening angle between photon and positron. No event lies in both of the signal regions.

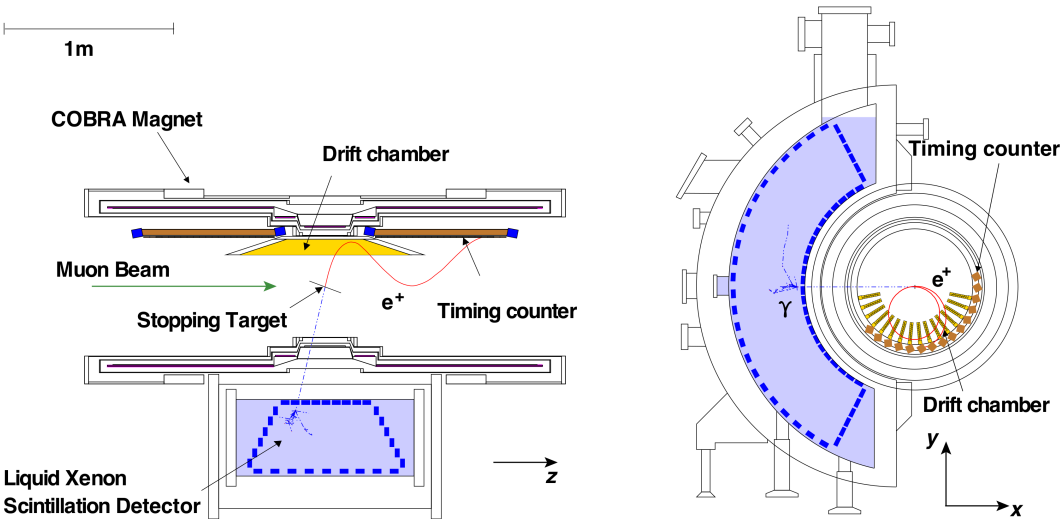

Figure 5: Sketch of the MEG detector [14].

At the moment, the MEG experiment undergoes an upgrade, called MEGII [15]. The positron tracker and timing detector are replaced and the liquid Xenon calorimeter is upgraded. The thus improved energy, angular and timing resolution allows for running at higher muon rates. MEGII has a prospected sensitivity of $5 \cdot 10^{-14}$ in 3 years data taking, about one order in magnitude better than MEG.

2.4 The Decay $\mu \to eee$

In the case of $\mu \to eee$, the **signature** is two positrons and one electron that appear coincidently from a common vertex. Studying muon decays at rest, the momenta of the electrons sum up to zero whereas the sum of the energies equals the muon rest mass. The maximum momentum of a single electron is about 53 MeV.
One source of **background** is $\mu \to eee\nu\overline{\nu}$, as the neutrinos leave the detector unseen. It can be distinguished from the signal decay only because of the missing energy of the neutrinos. Therefore, a very good momentum resolution is crucial to suppress this background. This is illustrated in figure 8. Here, the branching ratio of $\mu \to eee\nu\overline{\nu}$ is integrated with a cut on the missing energy $m_\mu - E_{\text{tot}} = m_\mu - \sum_{i=1}^{3} \vec{p}_i$. The missing energy needs to be known with better than 1 MeV precision in order to suppress this background below the aimed at sensitivity level.
Also $\mu \to eee$ searches have to cope with accidental background. These are usually coincidences of one or two positrons from the dominant Michel decay and an electron or electron-positron pair from Bhabha scattering or photon conversion. Also a positron track can look like an electron if the track is reconstructed in the opposite direction. Additionally to a good momentum resolution — in general these combinations do not necessarily fulfill the criteria on momentum and energy — accidental combinations can be suppressed by a good timing and vertex resolution.
The decay $\mu \to eee$ has been last investigated by the SINDRUM experiment [16] in 1988. No signal event was found and an upper limit on the branching ratio was set at $\text{BR} < 1.0 \cdot 10^{-12}$ at 90% confidence level.

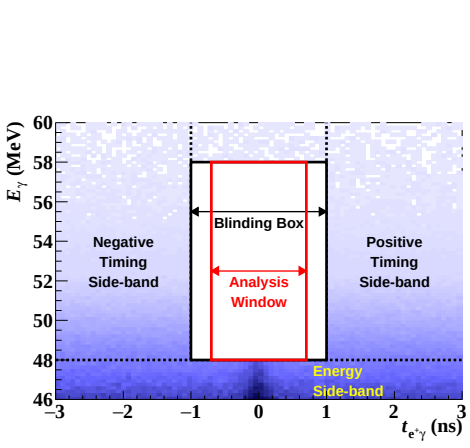

(a) Blinding box and side-bands.

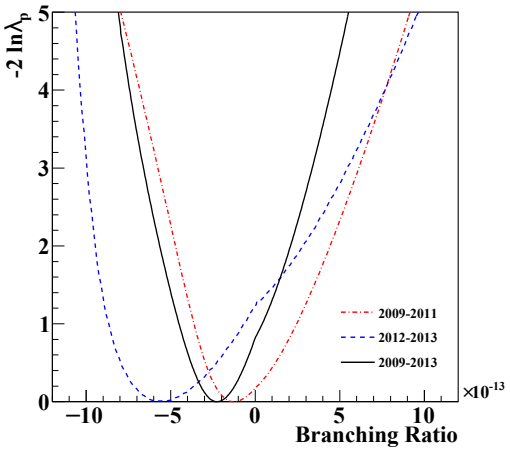

(b) Negative log-likelihood ratio as a function of the branching ratio for $\mu \to e\gamma$.

Figure 6: Combination of blind and maximum likelihood analysis of the MEG data [14].

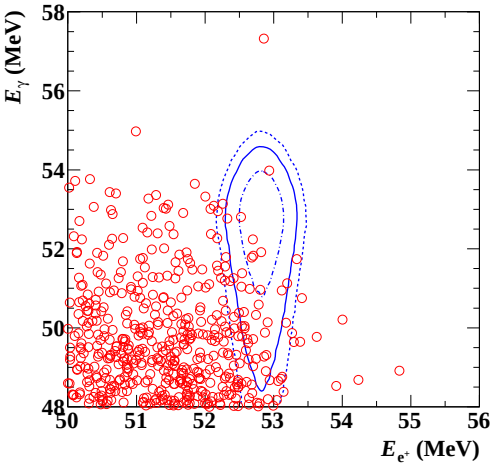

(a) Photon and positron energies.

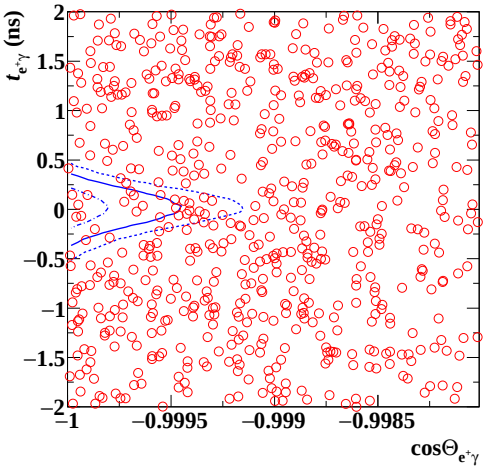

(b) Time difference and opening angle.

Figure 7: Distibution of events in the MEG experiment. The signal PDF contours at 1σ, 1.64σ and 2σ signal regions are indicated [14].

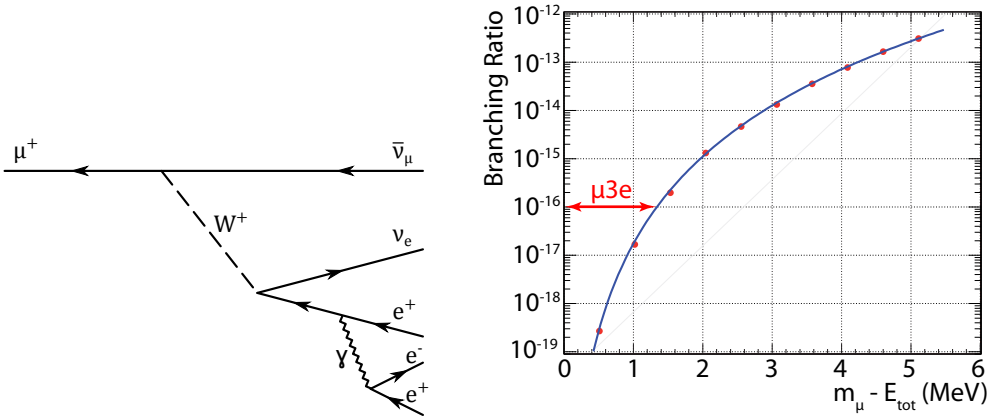

Figure 8: Integrated branching ratio for $\mu \rightarrow eee\nu\bar{\nu}$ for various cuts on the missing energy [17].

3 The Mu3e Experiment

The Mu3e experiment [18–20] aims to improve the SINDRUM results by three to four orders of magnitude. The following discussions will focus on phase I of Mu3e aiming at a sensitivity of 10^{-15} in branching ratio, but the majority of the concepts presented will also be valid for the phase II with a final sensitivity of 10^{-16}.

There are a couple of challenges in order to reach these sensitivities. First of all, as a **high number of muon decays** has to be observed, it is necessary to operate at very high muon stopping rates. Phase I will be located at the most intense muon beamline at PSI with a rate of $10^8\,\mu/s$ stopped on target. Such high rates are necessary to perform the experiment on a reasonable time scale. For phase II, rates in the excess of $10^9\,\mu/s$ become necessary. The PSI is investigating on a new beamline that is able to provide this rate.

A high muon stopping rate comes along with a **high track rate** in the detector. Thus, the tracking detector needs to have low dead times and a high granularity to counteract occupancy.

In addition, the **acceptance** of the detector should be as large as possible. Acceptance losses are caused by the geometrical acceptance as a result of non-instrumented areas (e. g. close to the beam pipe) and by a limited energy coverage.

On the other hand, the sensitivity reach of the experiment depends on the capability to distinguish signal events from background. Mu3e will be performed **background-free** meaning that the amount of background in the signal region can be suppressed well below the aimed sensitivity level. For this purpose a **high momentum, vertex and timing resolution** is necessary to control and suppress background from $\mu \rightarrow eee\nu\bar{\nu}$ and from accidental combinations.

In Mu3e, the decay electrons have momenta of up to 53 MeV. Thus, the momentum resolution is dominated by **multiple scattering** of the decay electrons in the surrounding material, hence the amount of material in the experiment has to be kept at a minimum.

The various parts of the Mu3e experiment are described in the following.

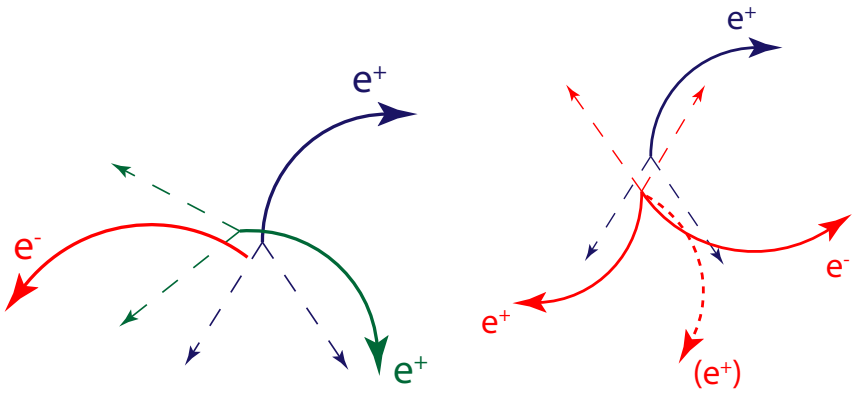

(a) Combination of two e^+ from $\mu \rightarrow e\nu\bar{\nu}$ with an e^- for example from Bhabha scattering.

(b) Combination of a e^+ from $\mu \rightarrow e\nu\bar{\nu}$ and an e^+e^- pair from $\mu \rightarrow eee\nu\bar{\nu}$.

Figure 9: Accidental background for $\mu \rightarrow eee$.

3.1 The Target

The target is a hollow double cone made out of Mylar foil with a thickness of about 80 µm. As the muons have a momentum of about 28 MeV, this in combination with a degrader in the beam line is enough to achieve a **high stopping fraction**. The target is about 10 cm long with a radius of 1.9 cm. The radius is chosen to match the width of the muon beam. The particular target shape distributes the muon stops and thus decay vertices over a larger surface. This simplifies the **vertex separation** to some extent. In addition, it is beneficial if the electrons have to transverse as little target material as possible in order not to be distorted by multiple scattering and to lower the chances for Bhabha scattering.

3.2 The Tracking Detector

Tracking in the Scattering-Dominated Regime Charged particles traversing material are deflected at the material's nuclei by **elastic Coulomb scattering**. As a result, the particles leave the material under an angle compared to the incident direction. The scattering angle θ_{MS} for a particle with velocity β, momentum p, and charge z in terms of electron charges e traversing a material with thickness x and radiation length X_0 is [1]

$$\theta_{\text{MS}} = \frac{13.6\,\text{MeV}}{\beta p} z \sqrt{\frac{x}{X_0}} \left(1 + 0.038 \ln\left(\frac{x}{X_0}\right)\right) . \tag{3}$$

As can be easily seen in equation 3, the deflection is stronger for particles with low momenta. Thus, tracking in the case of low momentum particles (*scattering dominated regime*) has to be treated differently than in the case of high momentum particles (*spatial resolution regime*).
In the spatial resolution regime, the particle trajectories are mostly straight tracks (see figure 10a). The tracking precision can be improved by improving the spatial resolution of the tracking detector (e. g. smaller pixel sizes) and by adding more measurement points. If multiple scattering is dominating on the other hand, the spatial resolution is not as important but the overall material in the

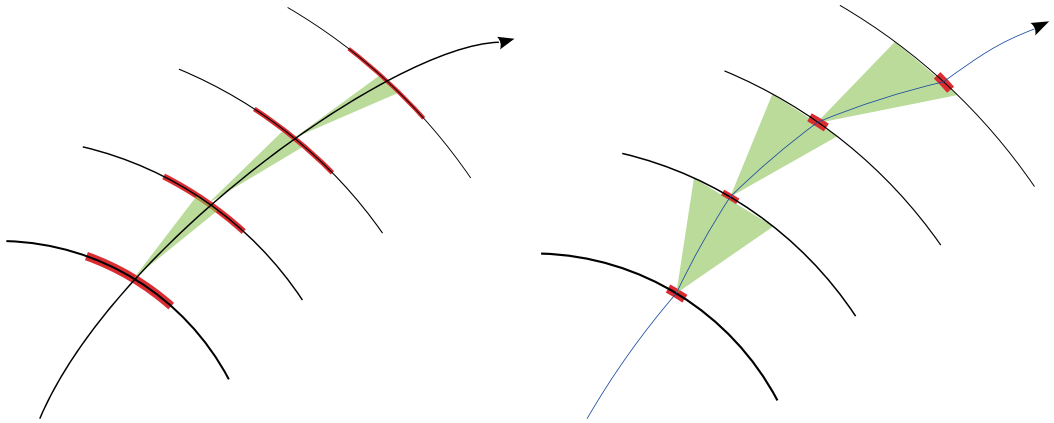

(a) Spatial regime.

(b) Scattering regime.

Figure 10: Tracking in a spatial resolution and scattering dominated regime.

active detector volume is (see figure 10b). Thus, it might not be beneficial to add additional measurement points as these come at the cost of additional detector material.

The Mu3e Silicon Pixel Tracker In Mu3e, the momentum and sign of the charge of the electrons is measured via the curvature of the tracks in a magnetic field. A homogeneous solenoidal field of 1 T is applied along the z-axis of the detector. Particle identification is not necessary as all detected particles can only be electrons.
The tracking detector is built up of **thin pixel sensors cylindrically arranged around the beam axis**. Only four layers of pixel detectors are used in order not to add too much material.
For a good **vertex resolution**, it is desirable to have the innermost pixel layer as close to the target as possible. The minimum radius is determined by the target dimensions and by the beam profile. There are two vertex layers with length 12 cm and radii of about 2.3 cm and 3.0 cm.
The relative momentum resolution for scattering dominated regime scales with the inverse of the lever arm Ω (see figure 11a)

$$\frac{\sigma_p}{p} \propto \frac{\theta_{\mathrm{MS}}}{\Omega} \,. \tag{4}$$

Thus, a tracking detector design with a **large lever arm** will give a better performance. But this results in a larger radius for the outer layer which affects the **acceptance for low momentum particles**. This is illustrated in figure 12. In Mu3e, there are two outer pixel layers with length 34 cm and 36 cm and radii 7.4 cm and 8.6 cm.
As a magnetic field is applied, the electrons will eventually return to the outer pixel layers following their helical trajectory. These are called *recurler*. The lever arm between the two measurement points in the outer layer is very large, for many momenta in the range of a half-turn. This is particularly good for the momentum resolution as after a half-turn the effect of multiple scattering cancels to first order (see figure 11b). In order to increase the acceptance for recurlers, the Mu3e detector has the shape of a narrow long tube (see figure 13). The central detector station with vertex

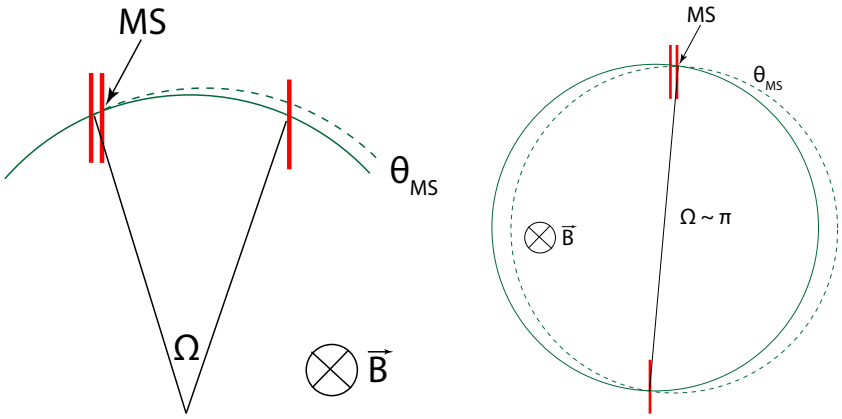

(a) Medium-sized lever arm. (b) Lever arm of about one half-turn.

Figure 11: Effects of multiple Coulomb scattering.

and outer pixel layers is extended upstream and downstream by so-called recurl stations equipped each with two layers of pixel sensors with the same radii as the central outer layers.
For the pixel sensors a high efficiency and low noise rate is required, as well as a high-rate capability. The pixel size is $80 \times 80\mu m^2$. Most importantly, the pixel sensors need to be very thin. For Mu3e, high-voltage monolithic active pixel sensors (HV-MAPS) are chosen [21–23]. Ionisation charges of traversing particles are detected in a pn-junction which is reversely biased with a voltage of about 85 V. As the active detection volume of the pn-junction is rather thin with about 15 µm, thinning down to a thickness of 50 µm becomes possible. In the HV-MAPS technology, readout circuitry for hit detection and digitisation can be directly implemented on the sensor chip eliminating the need for an additional readout chip. This way, one pixel layer consisting of the sensor itself as well as the electrical supply and mechanical support accounts for only 0.115 % of a radiation length.
As the sensors dissipate heat, the detector needs to be cooled. This is done with a gaseous helium flow as also scattering in the gas deteriorates the momentum resolution.

3.3 The Timing Detector

The timing resolution of the tracking detector itself is not good enough to sufficiently suppress accidental background. Figure 14 shows the amount of tracks in a readout frame of 50 ns. With additional timing information, single tracks can be identified. In addition to the improved timing resolution for **suppressing accidental combinations**, the timing information is also used to identify the **sign of the charge** of the particle.
Mu3e foresees two timing detector systems. In the central detector volume where the material amount is crucial only a thin timing detector can be installed. Here, the timing detector is made of three to four layers of scintillating fibres. It is located within the second and third pixel layer at a radius of 6.4 cm and with a length of 28 cm.
In the recurl stations, the timing detector is located underneath the pixel layer. Here, the amount of material used is no longer an issue. Therefore, scintillating tiles are chosen as timing detectors for the recurl stations.
Both timing detector systems use silicon photo-multipliers for the detection of the scintillation

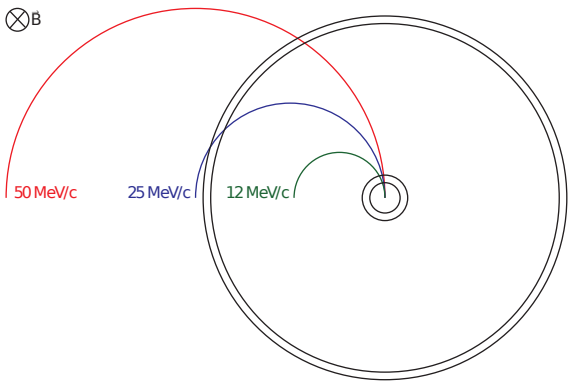

(a) Larger radius.

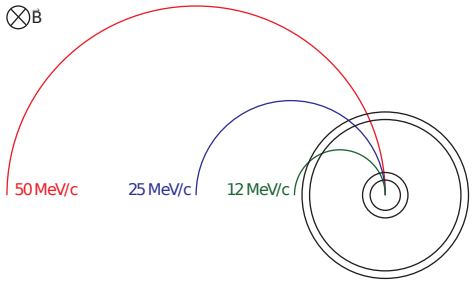

(b) Smaller radius.

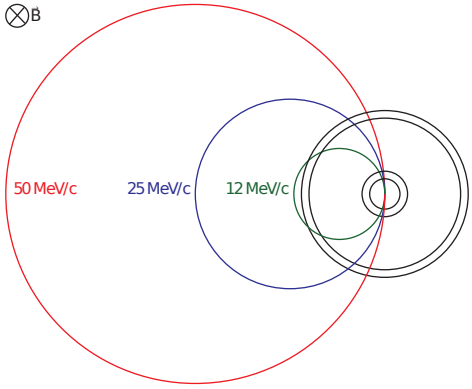

(c) Detecting recurling particles.

Figure 12: Influence of the radius of the outer tracking layers on the acceptance and lever arm of the momentum measurement.

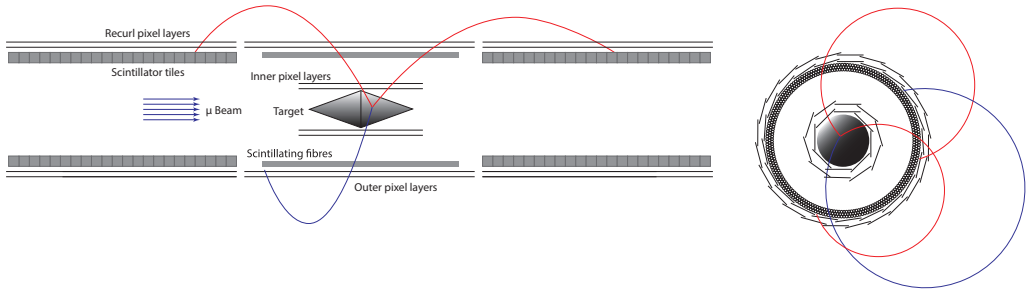

(a) Longitudinal view.

(b) Transverse view.

Figure 13: The Mu3e detector for phase I.

light and a custom-designed ASIC, the MuTRiG [24], for readout and digitisation.

3.4 Data Acquisition

Mu3e operates without a hardware trigger. All detector sub-systems continuously stream zero-suppressed data to the data acquisition chain. The data rate accumulates to $\leq$ 100 Gbit/s in phase I. A filter farm reduces this data rate to reasonable $\sim$ 100 MB/s by selecting only $\mu \rightarrow$ eee candidates which are then stored on disk for offline analysis. For this, is it necessary to perform a fast track fit at the filter farm level. Only events that contain at least two positron and one electron track for which a common vertex can be found are kept.

3.5 Reconstruction and Vertex Finding

The track reconstruction has desirably a high precision and efficiency and a low rate for wrongly reconstructed tracks. One particular difficulty in Mu3e are recurling particles that only have little momentum in longitudinal direction. These particles do several turns in the central detector which are difficult to seperate from each other. For the implementation on the filter farm the reconstruction algorithm needs to be very fast. In Mu3e, a fast three-dimensional track fit based on multiple scattering is used.
In the first track finding step, triplets are formed from hits in the three inner pixel layers and the scattering angles at the middle hit are fitted. A fourth hit is added by building a triplet from the hits in layer two to four and then joining the two triplets. This is done by minimizing the sum of the χ^2 functions with respect to the scattering angles. These tracks consist of four hits and are called *short tracks*. They are used in the online event selection.
In the offline analysis, more refined reconstruction algorithms can be employed. The short tracks are extended to *long tracks* whenever possible. Long tracks make use of recurlers. They are built from short tracks by adding two hits in the outer layers, or even four hits for particles with little longitudinal momentum hitting the vertex layers again.
The vertex is fitted for combinations of two positron and one electron track. The scattering angles at the innermost layer are varied in order to have three tracks intersect in one common vertex.

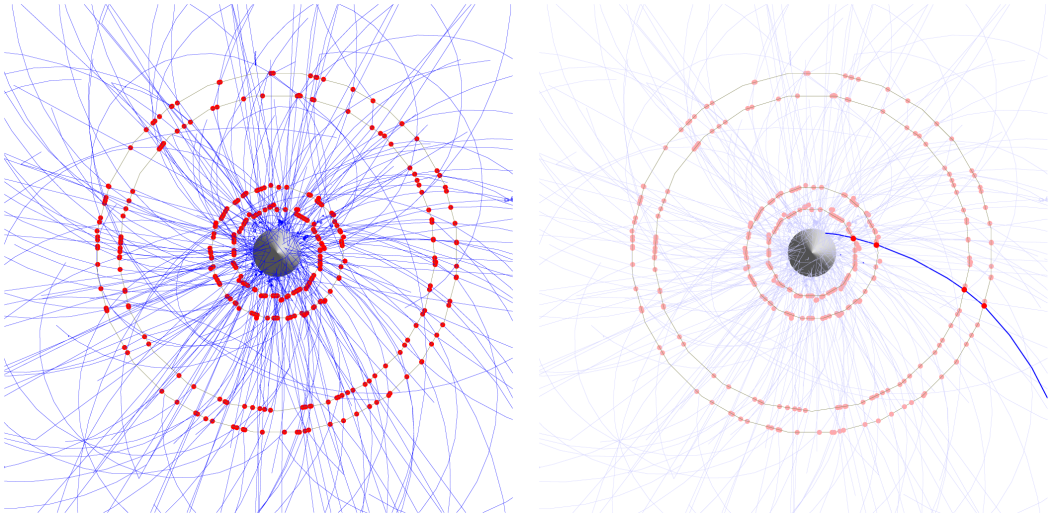

(a) Tracks in a 50ns readout frame.

(b) Using additional timing information.

Figure 14: Using additional timing information from the timing detectors helps to single out individual tracks.

3.6 Sensitivity in Phase I

The sensitivity is estimated using a Geant4 based detector simulation and reconstructing tracks and vertices from the obtained data.
Signal events are simulated assuming a phase-space distribution. The geometrical acceptance for all three tracks being reconstructable is about 42.2%. This is reduced further by reconstruction and applying cuts. If three recurling tracks are required — which gives the best momentum resolution — the overall efficiency is 18.4%.
Background stems from the radiative decay with internal conversion and from accidental combinations. Both can be suppressed by kinematic constraints. The latter is also suppressed by timing and vertexing. Figure 15a shows the reconstructed mass of the three electrons for signal and internal conversion events. No accidental background event lies in the signal region after cuts so that an upper limit is given. Mu3e can run background-free in phase I for at least $2.5 \cdot 10^{15}$ stopped muons or 300 days of data taking at $10^8 \mu/s$ and is capable to achieve a sensitvity of BR $\approx 5 \cdot 10^{-15}$ at 90% confidence level (see figure 15b).

4 Physics Studies with the Mu3e Experiment

The Mu3e experiment will observe a large number of muon decays — about 10^{15} in the first phase and more than 10^{16} in the second phase — with a detector with large geometrical acceptance and a high momentum resolution. This offers the possibility to investigate a variety of physics channels. With a couple of $\mu \to eee$ events it becomes possible to discriminate different effective operators. But also searches for decays of the type $\mu \to e X$ are possible, as well as for muon decays in which a dark photon is emitted. With modifications to the detector, $\mu \to e\gamma$ can be studied. In addition, pion decays like $\pi \to ee\gamma$ can be investigated when operating at a pion beam line.

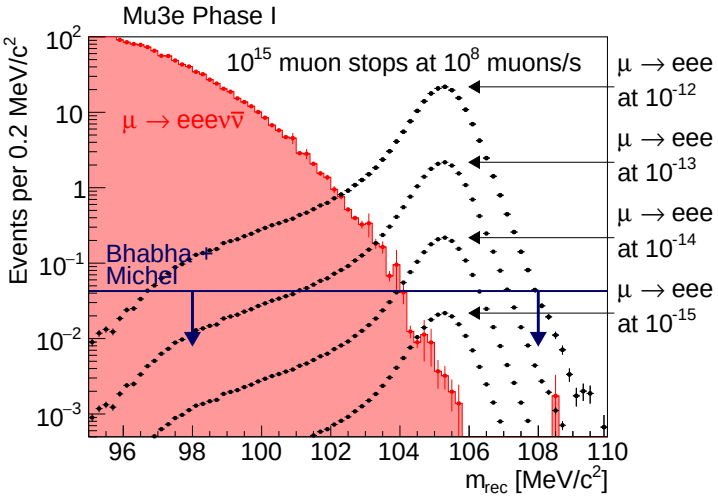

(a) Invariant mass of the three electrons for signal and background.

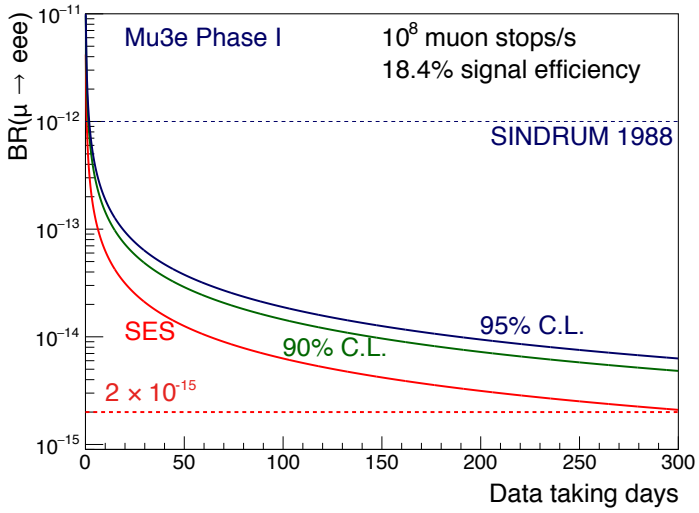

(b) Prospected sensitivity.

Figure 15: Sensitivity to $\mu \to eee$ of the Mu3e phase I detector.

In the following, the $\mu \to eee$ decay in effective theories and the decay $\mu \to e\,X$ are discussed.

4.1 $\mu \to eee$ with Effective Operators

In Mu3e as well as in the preceding SINDRUM experiment, the sensitivity of the experiment is derived for $\mu \to eee$ events evenly distributed in phase-space making no assumptions on the potential physics mediating the decay. Different physics models however lead to diverse kinematics of the decay electrons, and thus are detected with different efficiencies as a result of the finite acceptance of the detector and the vertex reconstruction efficiency. This can be studied for instance in the context of **effective theories**.
In figure 16, Dalitz plots of the invariant mass squared of the two electron-positron systems are shown for phase-space decays and for decays mediated by either a dipole-like operator or a four-fermion contact interaction. The operators are chosen as in equation 2 [7, 11] (see also figure 4).
For **phase-space decays**, the events are evenly distributed in the Dalitz plot. However, the detector response is not completely homogeneous over the whole accessible phase space. Figure 16b shows the efficiency of finding a vertex for phase-space distributed decays, meaning that all three tracks are within the acceptance, are reconstructed and a vertex could be found. For the vertex fit, all three tracks are requested to be recurlers as this ensures the best momentum and thus mass resolution and allows for efficient background suppression. The edges of the triangle are cut and in these areas the efficiency is lower than in the remaining area. This is mainly due to the geometrical acceptance as in these cases one of the decay electrons has a low momentum.
In the case of **dipole interactions**, it is preferred to have at least one electron-positron pair with a very small invariant mass — just as in photon conversion. This results in having many events lying in regions outside of the detector acceptance. In addition, the vertex fit is less likely to converge for topologies with two almost parallel tracks. This reduces the efficiency for dipole-like interactions further.
The picture changes significantly for **four-fermion interactions**. For the chosen operators, the center of the Dalitz plot with invariant masses of equal size for both electron-positron systems is preferred, and fewer events lie outside of the acceptance.
It turns out, that the **efficiency** for four-fermion interaction is with 17.1 % even slightly higher than for the phase space decay with 15.4 %. For dipole interactions, the efficiency is however noticeably reduced with 8.9 %[1].
This effects also the prospected **sensitivity**. After $2.5 \cdot 10^{15}$ observed muon stops in the Mu3e experiment, the single-event-sensitivity (SES) to phase space distributed $\mu \to eee$ signals is $2.6 \cdot 10^{-15}$, and the 90 % confidence level (CL) is at BR $< 6.0 \cdot 10^{-15}$, whereas the sensitivity is $2.3 \cdot 10^{-15}$ SES and BR $< 5.3 \cdot 10^{-15}$ at 90 % CL for four-fermion interaction, respectively. For dipole interaction, the SES is at $4.5 \cdot 10^{-15}$ and the 90 % CL at BR $< 10.4 \cdot 10^{-15}$ (see figure 17).

4.2 Searches for the Decay $\mu \to e\,X$

In addition to the decay $\mu \to eee$ also other decay channels can be investigated with the Mu3e experiment, one of which being the decay $\mu^+ \to e^+ X^0$ with the neutral light boson X^0 leaving the detector unobserved. Such a particle is for instance motivated by **familons** [25]. These are (pseudo-) Nambu-Goldstone bosons that arise from introducing a spontaneously broken flavour symmetry. The familons are emitted in flavour-changing decays e. g. of the muon.

[1] Please note, that slightly different cuts are applied compared to the results presented in section 3.6 yielding different efficiencies.

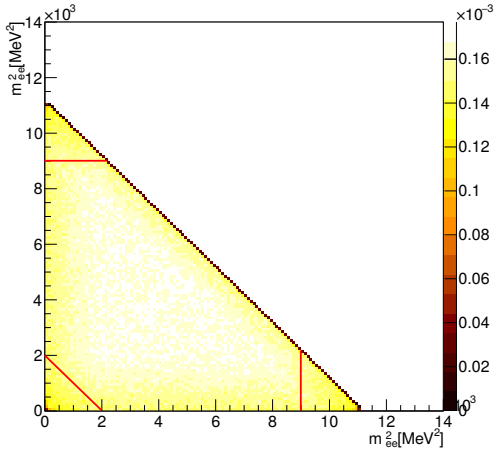

(a) Phase space decay.

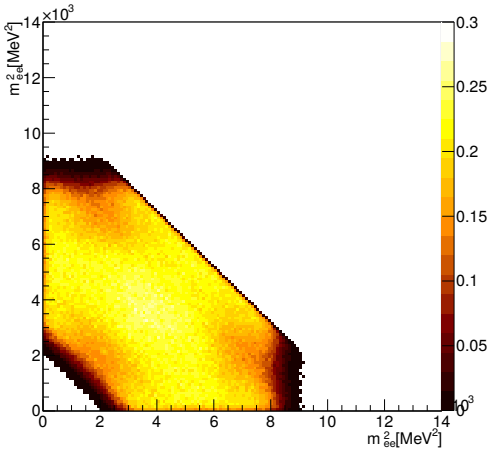

(b) Efficiency of vertex finding for the phase space decay.

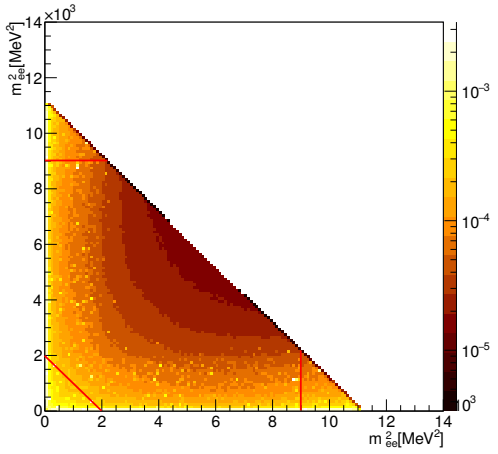

(c) Dipole operator (please note the logarithmic scale).

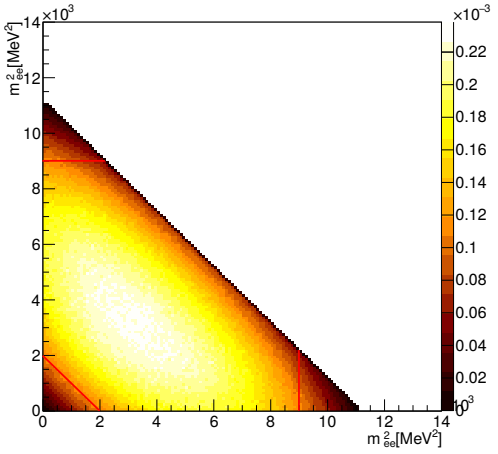

(d) 4-fermion operator.

Figure 16: Dalitz plots of the invariant masses squared of the electron-positron system for different effective operators. The data shown is truth information. The geometrical acceptance is indicated by the red lines.

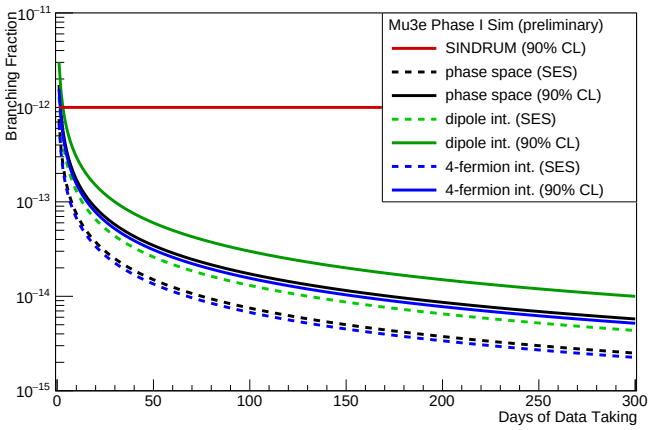

Figure 17: Prospected sensitivity to $\mu \to eee$ of the Mu3e phase I detector operating at $1 \cdot 10^8 \mu/s$ for phase-space signals and signals mediated via a dipole and a four-fermion effective operator. Three recurling tracks are requested in the vertex fit. The experimental limit given for the SINDRUM experiment corresponds to phase-space signals [16].

The currently most stringent bound on $\mu^+ \to e^+ X^0$ with a **massless** boson is at BR $< 2.6 \cdot 10^{-6}$ at 90% CL [26]. For such searches, decays at rest of highly polarised antimuons are investigated. One searches for an excess of positrons with an energy of half the muon rest mass ideally in a direction opposite to the muon spin (see figure 18).
In the case of Mu3e, a search for massless X^0 is not feasible as the edge of the Michel spectrum itself is affected by alignment and calibration. In addition, the accessible muon polarisation at the beamline of Mu3e is with about 85% not high enough to allow for searches in areas opposite to the muon spin. In figure 19, the effect of an increased radius of the pixel detector layers is shown as an example for mis-alignment. The edge of the Michel spectrum is shifted whereas the effect on the continuous spectrum is moderate. The shift of the Michel edge is smaller in the case of long tracks as these have a better momentum resolution and thus the edge is steeper in the reconstructed momentum spectrum.
Although massless X^0 cannot be investigated, searches for **massive** X^0 are possible. The current best limit is from the TWIST experiment which excludes massive X^0 of up to 80 MeV at a BR $< 9 \cdot 10^{-6}$ at 90% on average [27].

As $\mu^+ \to e^+ X^0$ is a two-body decay, it would show up as an **excess on top of the momentum spectrum** of the positrons from SM muon decays (see figure 20a). The position of the peak is purely determined by the mass m_{X^0}

$$p_e = \sqrt{\left(\frac{m_\mu^2 - m_{X^0}^2 + m_e^2}{2m_\mu}\right)^2 - m_e^2}\,. \tag{5}$$

The largest m_{X^0} that can be studied is determined by the acceptance for low momentum particles. Positrons below about 10 MeV cannot reach the fourth pixel layer and are thus not reconstructed.

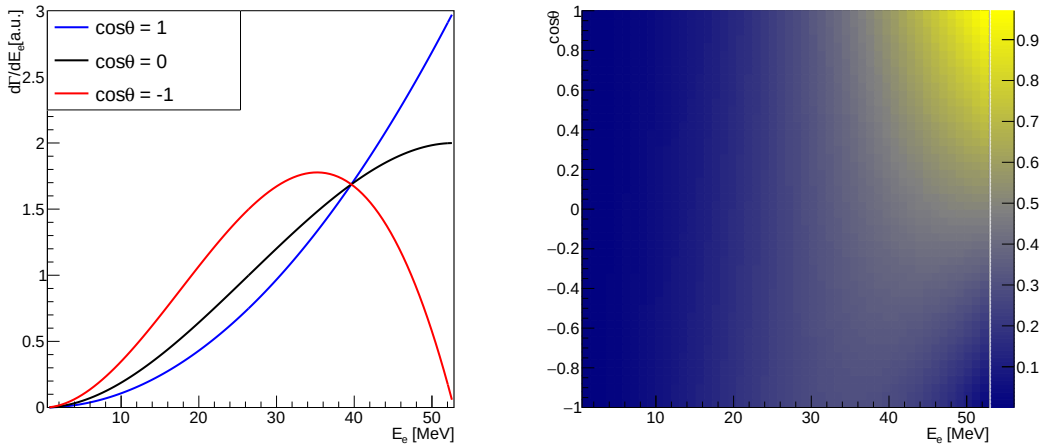

Figure 18: Energy spectrum of the positron in Michel decays for the angle θ between the positron momentum and the muon spin.

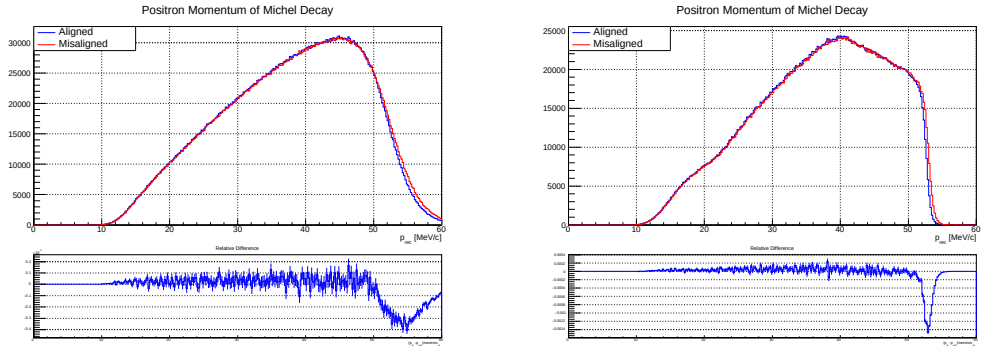

(a) Short tracks.

(b) Long tracks.

Figure 19: Effect of misalignment on the reconstructed positron momentum spectrum. The radius of the pixel layers is increased by 0.8%. Plots by courtesy of U. Hartenstein.

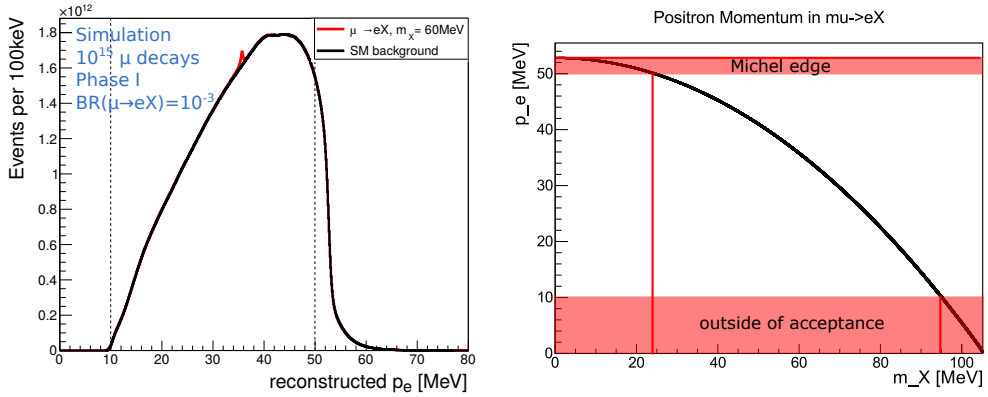

(a) $\mu \rightarrow e X$ signature.

(b) Range of m_{X^0}.

Figure 20: Possible signature from $\mu \rightarrow e X$ decays in the momentum spectrum of positrons from muon decays and the accessible mass range.

Omitting the Michel edge by requiring $p_e < 50\,\text{MeV}$ gives the lower edge of the mass scale. Thus, m_{X^0} in the range of 25 MeV to 95 MeV can be investigated with Mu3e (see figure 20b).

The **sensitivity** that can be achieved depends on the number of observed muon decays and the momentum resolution. In Mu3e it is not possible to keep every event when running at high muon stopping rates, but all tracks are reconstructed online before possible $\mu \rightarrow eee$ candidates are selected on the filter farm. It is possible to keep a **histogram of the momenta** obtained in the **online reconstruction** for $\mu \rightarrow e X$ searches. The baseline design of phase I foresees to reconstruct **short tracks** from four hits in the central detector station. The momentum resolution for these tracks ranges from 0.5 MeV to 3.0 MeV (see figure 21a). This is the starting point for the sensitivity studies.
A large sample of SM muon decays as well as of $\mu \rightarrow e X$ decays is simulated and reconstructed. In order to avoid ambiguities in the reconstruction caused by recurling tracks, positron tracks that are emitted very perpendicular to the muon beam are omitted. The obtained histograms as can be seen in figures 22a and 22b are used as probability density functions (p.d.f.s) for **Toy Monte Carlo studies**. A large sample of events is drawn from the background p.d.f. and subsequently fitted assuming background and signal with the signal fraction as free parameter (see figure 22c). Repeating this procedure many times yields a distribution of the signal fraction as shown in figure 22d. The 90 % CL for instance is derived by determining the signal fraction for which 90 % of the fitted signal fractions lie below this value. Assuming $1 \cdot 10^{15}$ observed muon decays, the Mu3e experiment is capable to measure $\mu \rightarrow e X$ decays with branching ratios in the range of $1 \cdot 10^{-7}$ to $5 \cdot 10^{-7}$ at 90 % CL for m_{X^0} from 25 MeV to 95 MeV (see figure 23).
Although not foreseen in the baseline design, with the progress in the technology of graphics processing units it might become possible to reconstruct also **long tracks** already online. $\mu \rightarrow e X$ searches would highly benefit from the improved momentum resolution of about 0.1 MeV to 0.45 MeV. Repeating the Toy Monte Carlo studies with reconstructed long tracks yields branching ratios in the range of around $1 \cdot 10^{-8}$ at 90 % CL (see figure 24) — about an order of magnitude improvement compared to reconstructing short tracks.

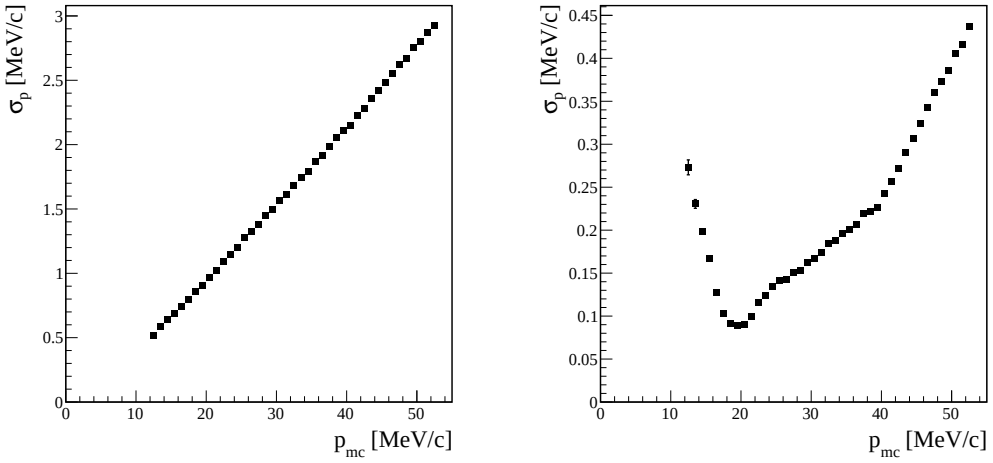

(a) Short tracks.

(b) Long tracks.

Figure 21: Momentum resolution for reconstructed short and long tracks.

Figure 25 shows the prospected 90% CL limits for both reconstructions in comparison to the results of the TWIST experiment. As a result of the large number of muon decays to be observed, the Mu3e experiment can improve the current limits by about one order of magnitude over a large mass range, and even by two orders if long tracks are reconstructed.
In general, the X^0 could also have flavour-diagonal couplings. It would thus appear in the decay $\mu \to eee$. With a handful of events, m_{X^0} could be derived from the invariant mass of the electron-positron system.

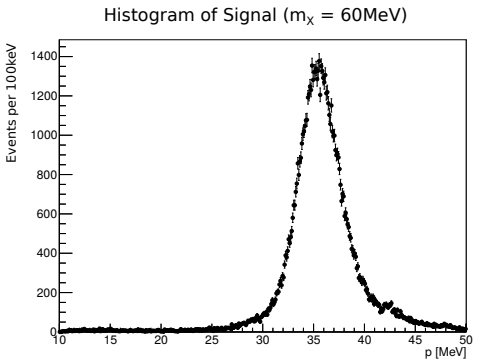

(a) Signal histogram.

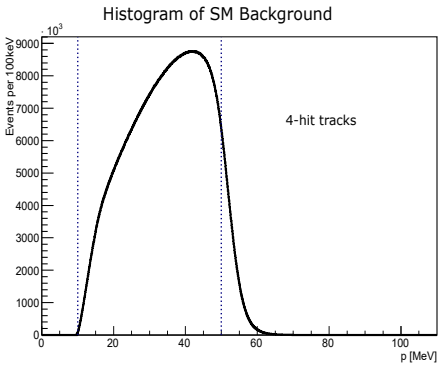

(b) Background histogram.

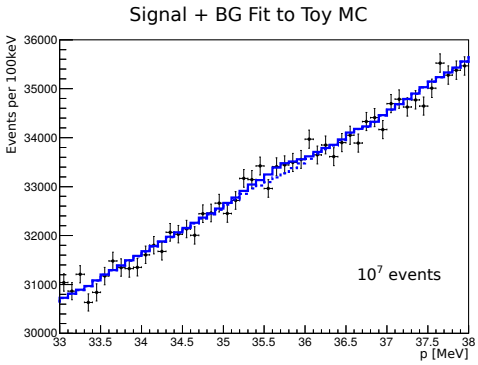

(c) Fit of signal plus background zoomed in around the peak.

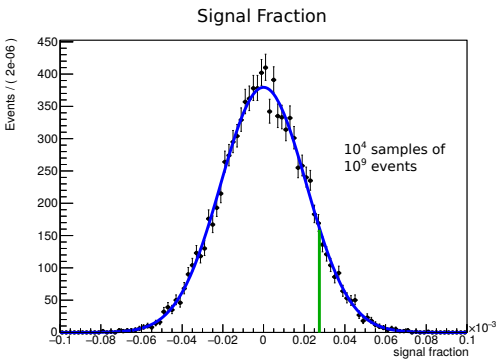

(d) Distribution of fitted signal fraction.

Figure 22: Estimating the sensitivity to $\mu \rightarrow e\,X$ decays with Toy Monte Carlo studies.

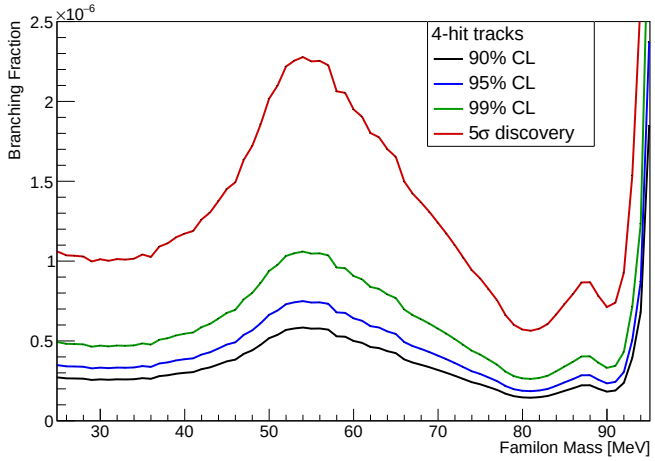

Figure 23: Prospected sensitivity to $\mu \rightarrow e X$ decays assuming $1 \cdot 10^{15}$ observed muon stops. The positrons are reconstructed as short tracks.

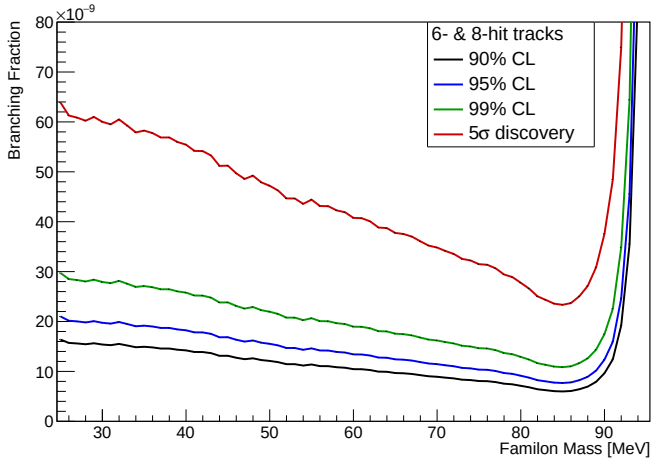

Figure 24: Prospected sensitivity to $\mu \rightarrow e X$ decays assuming $1 \cdot 10^{15}$ observed muon stops. The positrons are reconstructed as long tracks.

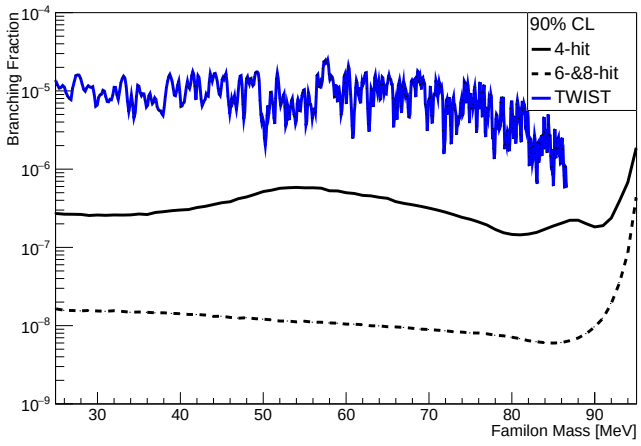

Figure 25: Prospected 90% confidence limit on $\mu \to e X$ decays assuming $1 \cdot 10^{15}$ observed muon stops in the Mu3e experiment for positrons reconstructed as short or long tracks, respectively. The upper limits by the TWIST experiment are shown for comparison [27]. TWIST results by courtesy of R. Bayes.

5 References

[1] C. Patrignani et al. "Review of Particle Physics." In: *Chin. Phys.* C40.10 (2016), p. 100001. DOI: 10.1088/1674-1137/40/10/100001.

[2] A. Hillairet et al. "Precision muon decay measurements and improved constraints on the weak interaction." In: *Phys. Rev.* D85 (2012), p. 092013. DOI: 10.1103/PhysRevD.85.092013. arXiv: 1112.3606 [hep-ex].

[3] G. W. Bennett et al. "Final Report of the Muon E821 Anomalous Magnetic Moment Measurement at BNL." In: *Phys. Rev.* D73 (2006), p. 072003. DOI: 10.1103/PhysRevD.73.072003. arXiv: hep-ex/0602035 [hep-ex].

[4] Thomas Blum, Achim Denig, Ivan Logashenko, Eduardo de Rafael, B. Lee Roberts, Thomas Teubner, and Graziano Venanzoni. "The Muon (g-2) Theory Value: Present and Future." In: (2013). arXiv: 1311.2198 [hep-ph].

[5] R. Abramishvili et al. "COMET Phase-I Technical Design Report." In: (2016).

[6] L. Bartoszek et al. "Mu2e Technical Design Report." In: (2014). arXiv: 1501.05241.

[7] Andre de Gouvea and Petr Vogel. "Lepton Flavor and Number Conservation, and Physics Beyond the Standard Model." In: *Prog. Part. Nucl. Phys.* 71 (2013), pp. 75–92. DOI: 10.1016/j.ppnp.2013.03.006. arXiv: 1303.4097 [hep-ph].

[8] S. T. Petcov. "The Processes mu -> e Gamma, mu -> e e anti-e, Neutrino' -> Neutrino gamma in the Weinberg-Salam Model with Neutrino Mixing." In: *Sov. J. Nucl. Phys.* 25 (1977). [Erratum: Yad. Fiz.25,1336(1977)], p. 340.

[9] Samoil M. Bilenky, S. T. Petcov, and B. Pontecorvo. "Lepton Mixing, mu −> e + gamma Decay and Neutrino Oscillations." In: *Phys. Lett.* 67B (1977), p. 309. DOI: 10.1016/0370-2693(77)90379-3.

[10] William J. Marciano, Toshinori Mori, and J. Michael Roney. "Charged Lepton Flavor Violation Experiments." In: *Ann. Rev. Nucl. Part. Sci.* 58 (2008), pp. 315–341. DOI: 10.1146/annurev.nucl.58.110707.171126.

[11] Yoshitaka Kuno and Yasuhiro Okada. "Muon decay and physics beyond the standard model." In: *Rev. Mod. Phys.* 73 (2001), pp. 151–202. DOI: 10.1103/RevModPhys.73.151. arXiv: hep-ph/9909265 [hep-ph].

[12] A. Crivellin, S. Davidson, G. M. Pruna, and A. Signer. "Complementarity in lepton-flavour violating muon decay experiments." In: (2016). arXiv: 1611.03409 [hep-ph].

[13] J. Adam et al. "The MEG detector for $\mu^+ \to e^+\gamma$ decay search." In: *Eur. Phys. J.* C73.4 (2013), p. 2365. DOI: 10.1140/epjc/s10052-013-2365-2. arXiv: 1303.2348 [physics.ins-det].

[14] A. M. Baldini et al. "Search for the lepton flavour violating decay $\mu^+ \to e^+\gamma$ with the full dataset of the MEG experiment." In: *Eur. Phys. J.* C76.8 (2016), p. 434. DOI: 10.1140/epjc/s10052-016-4271-x. arXiv: 1605.05081 [hep-ex].

[15] A. M. Baldini et al. "MEG Upgrade Proposal." In: (2013). arXiv: 1301.7225.

[16] U. Bellgardt et al. "Search for the Decay mu+ −> e+ e+ e-." In: *Nucl. Phys.* B299 (1988), pp. 1–6. DOI: 10.1016/0550-3213(88)90462-2.

[17] Rashid M. Djilkibaev and Rostislav V. Konoplich. "Rare Muon Decay mu+ −> e+ e- e+ nu(e) anti-nu(mu)." In: *Phys. Rev.* D79 (2009), p. 073004. DOI: 10.1103/PhysRevD.79.073004. arXiv: 0812.1355 [hep-ph].

[18] A. Blondel et al. "Technical Design of the Phase I Mu3e Experiment." In: (in preparation).

[19] A. Blondel et al. "Research Proposal for an Experiment to Search for the Decay $\mu \to eee$." In: (2013). arXiv: 1301.6113 [physics.ins-det].

[20] A. Blondel et al. "Letter of Intent for an Experiment to Search for the Decay $\mu \to eee$." In: (2012).

[21] Ivan Peric. "A novel monolithic pixelated particle detector implemented in high-voltage CMOS technology." In: *Nucl. Instrum. Meth.* A582 (2007), pp. 876–885. DOI: 10.1016/j.nima.2007.07.115.

[22] I. Perić et al. "Overview of HVCMOS pixel sensors." In: *JINST* 10.05 (2015), p. C05021. DOI: 10.1088/1748-0221/10/05/C05021.

[23] Heiko Augustin et al. "The MuPix System-on-Chip for the Mu3e Experiment." In: *Nucl. Instrum. Meth.* A845 (2017), pp. 194–198. DOI: 10.1016/j.nima.2016.06.095. arXiv: 1603.08751 [physics.ins-det].

[24] H. Chen, K. Briggl, P. Eckert, T. Harion, Y. Munwes, W. Shen, V. Stankova, and H. C. Schultz-Coulon. "MuTRiG: a mixed signal Silicon Photomultiplier readout ASIC with high timing resolution and gigabit data link." In: *JINST* 12.01 (2017), p. C01043. DOI: 10.1088/1748-0221/12/01/C01043.

[25] Frank Wilczek. "Axions and Family Symmetry Breaking." In: *Phys. Rev. Lett.* 49 (1982), pp. 1549–1552. DOI: 10.1103/PhysRevLett.49.1549.

[26] A. Jodidio et al. “Search for Right-Handed Currents in Muon Decay.” In: *Phys. Rev.* D34 (1986). [Erratum: Phys. Rev.D37,237(1988)], p. 1967. DOI: 10.1103/PhysRevD.34.1967, 10.1103/PhysRevD.37.237.

[27] R. Bayes et al. “Search for two body muon decay signals.” In: *Phys. Rev.* D91.5 (2015), p. 052020. DOI: 10.1103/PhysRevD.91.052020. arXiv: 1409.0638 [hep-ex].